Visible-infrared two-dimensional Fourier-transform spectroscopy

Nadia Belabas, Manuel Joffre

Visible–infrared two-dimensional Fourier-transform spectroscopy

Nadia Belabas and Manuel Joffre

Laboratoire d'Optique et Biosciences, Institut National de la Santé et de la Recherche Médicale U451–Centre National de la Recherche Scientifique Unité Mixte de Recherche 7645–Ecole Polytechnique–École Nationale Supérieure des Techniques Avancées, 91128 Palaiseau Cedex, France

Received June 18, 2002

We report on a new class of optical multidimensional Fourier-transform spectroscopy associated with a visible excitation–infrared emission configuration, in which the emitted field results from second-order optical nonlinearities. This configuration is demonstrated on a phase-matched sample of known nonlinear response by coherent measurement of the mid-infrared field emitted after a femtosecond visible double-pulse excitation. © 2002 Optical Society of America

OCIS codes: 320.7110, 300.6300, 300.6420.

Optical spectroscopy techniques serve to provide knowledge of matter through the detection of radiated electric fields stemming from the oscillating electric dipole density, P, induced in a sample by the total incident field, E. In the perturbative regime, the response function of the material under study is entirely described by the set of its successive electrical susceptibilities, $\chi^{(n)}$, which are $n+1$-rank tensors. Conversely, the position, magnitude, and shape of the features of a complex map of $\chi^{(n)}$ hold all the information about existing couplings and inhomogeneities within the sample. They can in turn be related to the structural properties of crystals[1] and to couplings between bond stretches.[2–4] The latter can provide information about the three-dimensional structure of molecules and small peptides.[5,6] The dynamics of molecular environments can also be retrieved.[7] Outcomes of any optical measurement in the perturbative regime can of course be derived from these complex tensors. Complete measurement of the centerpiece $\chi^{(n)}$ is achieved only with multidimensional spectroscopy (nDSY). In practice, nDSY consists of measuring the field $E^{(n)}_{\text{emission}}$ radiated by the nth-order nonlinearity of a material as a function of p ($1 \le p \le n-1$) independent parameters to retrieve the nth-order nonlinear response $\Xi^{(n)}$ of the sample ($p = n-1$) or one of its projections ($p < n-1$). As the measured observable is the field $E^{(n)}_{\text{emission}}$ and not the ensemble-averaged electrical polarization, $P^{(n)}$, here we define the effective nth-order response $\Xi^{(n)}$ as

$$E^{(n)}_{\text{emission}}(\omega_1) = \int \Xi^{(n)}(\omega_2, \ldots, \omega_{n+1}) E(\omega_2) \ldots E(\omega_{n+1}) \delta\Big(\omega_1 - \sum_{i>1} \omega_i\Big) \mathrm{d}\omega_2 \ldots \mathrm{d}\omega_n , \quad (1)$$

where $\Xi^{(n)}$ incorporates not only macroscopic $\chi^{(n)}$ but also a propagation term [see Eq. (3), below] and, in the case $n > 2$, terms including $\chi^{(j)}$, where $j < n$ is associated with cascading effects. In summary, an nDSY measurement removes the integral in Eq. (1) by spreading the intricate and integrated emission $E^{(n)}_{\text{emission}}$ along p additional axes; for known E and $p = n-1$ this spreading allows retrieval of the map of $\Xi^{(n)}$ in n frequency dimensions.

The p parameters can be the wavelength of tunable continuous lasers,[4] but most experimental demonstrations are done through manipulation in the time domain with multiple-pulse Fourier-transform nonlinear spectroscopy[1–3,5,7] (nDFTSY), i.e., the optical analog of multiple quantum nuclear magnetic resonance.[8] In nDFTSY, the parameters are time delays τ_i, $2 \le i \le p+1$, in a sequence of femtosecond pulses E_i [$E = \sum_{i=2}^{p+2} E_i(t - \tau_i)$, $\tau_{p+2} = 0$]. In the case of $p = n-1$ studied experimentally below, the cross term of interest in Eq. (1) is

$$E^{(n)}_{\text{crossterm}}(\omega_1) = \int \Xi^{(n)}(\omega_2, \ldots, \omega_{n+1}) E_2(\omega_2) \exp(i\omega_2\tau_2) \times E_3(\omega_3) \exp(i\omega_3\tau_3) \ldots \delta\Big(\omega_1 - \sum_{i>1} \omega_i\Big) \mathrm{d}\omega_2 \ldots \mathrm{d}\omega_n . \quad (2)$$

In nDFTSY, the spectral map of $\Xi^{(n)}$ is retrieved with Fourier transforms of Eq. (2) relative to the τ_i Fourier conjugate of the ω_i.

The number of pulses, their wavelengths, their relative phases, and the beam geometry of the pulses within the exciting sequence are chosen according to the physics under study in the sample [i.e., according to the process involved in $\Xi^{(n)}$]: The second-order nonlinearity of noncentrosymmetric samples is probed with only two pulses,[1] in contrast with centrosymmetric and in particular liquid samples[2,3,5,7] ($n = 3, 5$), which are active only at the $\chi^{(3)}$ level. Electronic couplings are addressed in the visible[1,7]; vibrational couplings, in the infrared[3,5] or in the visible via Raman scattering.[2] Noncollinear geometry or a suitable set of phases of the exciting pulses can be used to isolate cross term (2). In all cases the phase between the exciting pulses must be stabilized as explained below.

Coherent detection of $E^{(n)}_{\text{emission}}(\omega_1)$ is necessary as both the amplitude and the phase of this field are required for computing the Fourier transforms. One can then use either Fourier-transform spectral interferometry[9] (multichannel detection) or time-domain interferometry with a local oscillator or reference field $E_1(t - \tau_1)$ (single-channel detector). In both cases one

0146-9592/02/222043-03$15.00/0

must be aware that Fourier transforms of unequally spaced data (because of either unjustified interpolation[10,11] or uneven time steps) result in distorted, aliased, and blurred maps. The stabilization and control of the time delays may be more demanding than the requirements for processing data from Fourier-transform spectral interferometry, but a time-domain interferometry setup is more versatile, as only one detector has to be replaced if one wishes to measure a new part of $\Xi^{(n)}$, i.e., a new spectral domain. Furthermore, time-domain interferometry is a widely used technique in the mid infrared, where multichannel detectors are not easily available.

In this Letter we present a two-dimensional ($p = 1$) Fourier-transform visible excitation–infrared emitted field measurement. In our experiment a visible pulse sequence excites through second-order nonlinear processes ($n = 2$) a low-frequency polarization that in turn radiates a mid-infrared field according to Eq. (1). The emitted field is measured with a broadband mid-infrared (center at 10 μm) reference field generated by optical rectification.[12] In contrast with previously reported all-infrared or all-visible experiments,[1–7] electronic and vibrational couplings can be simultaneously addressed in our visible–infrared configuration.

In practice (see the experimental layout in Fig. 1), the infrared emitter is excited by a sequence of two 16-fs 0.2-nJ 800-nm pulses delivered by a Ti:sapphire oscillator. The time delay τ_2 between the two visible (800-nm) pulses is the Fourier conjugate of a visible spectral axis (ω_2 or ω_3). The emitted field is measured in amplitude and phase by time-domain interferometry, i.e., through a linear correlation measurement with a reference infrared field, E_1. Note the rather unconventional geometry used in the experiment, the measured field being transmitted through the GaAs sample used for generation of the reference field through optical rectification. This approach, already discussed in detail previously,[12,13] allows dispersion compensation between the signal and the reference fields, since both undergo the same dispersion through propagation in the GaAs sample after the reference field has been generated in the first micrometer of the sample (one absorption length). We also checked that the free-carrier absorption in GaAs was kept at a negligible level so as not to change the spectrum of the signal field.

The time delay, τ_1, between the signal field and E_1 transforms into mid-infrared spectral variable ω_1. A two-dimensional Fourier transform of the cross term in the experimental data, with respect to both τ_1 and τ_2, thus yields $E_1^*(\omega_1)\Xi^{(2)}(\omega_2, \omega_2 + \omega 1)E_2^*(\omega_2)E_3(\omega_2 + \omega_1)$, from which the desired two-dimensional map of $\Xi^{(2)}$ can be deduced. It is noteworthy that the spectral phase of the reference and exciting fields is of no concern in this work, since we report only on the magnitude of the two-dimensional response $|\Xi^{(2)}|$, which can be directly deduced from the magnitude of the two-dimensional Fourier transform. For the same reason, the zero time delay between the reference and the signal field can be set arbitrarily.

However, as stated above, the validity of the retrieved $\Xi^{(2)}$ map yielded by a double Fourier transform of interferometric signal $S(\tau_1, \tau_2)$ depends strongly on the accuracy of the temporal axes τ_1 and τ_2. τ_1 is swept with a 0.1-μm step motor with no additional stabilization, as stability was *a priori* not an issue in the mid-infrared wavelength domain. τ_2 is actively stabilized by means of a 3-μm (10-fs) stroke piezoelectric transducer. The time–domain interferences Q_1 of a $\lambda_{\text{diode}} = 670$ nm laser diode propagating along the interferometer are used as a feedback signal, allowing precision of ~30 nm or 0.1 fs on τ_2. For resolution of $\delta\omega_2 = 1.75$ THz (58.3 cm^{-1}) on ω_2, τ_2 is scanned along 570.8 fs by means of a 0.1-μm step motor. To scan τ_2 while keeping track of the interference order (fringe number) of Q_1, we use a second time-domain interference signal, Q_2, with a phase differing from Q_1 by $\pi/2$. Q_2 is obtained by placement of a quarter-wave plate in one arm of the interferometer and detection of both polarizations at the output of a Glan polarizer.[14] Permanent tracking of Q_1 and Q_2 with a microcontroller makes possible accurate knowledge of τ_2 at any time. Even though the smallest time step along this visible τ_2 interferometer is λ_{diode}/c, since the central wavelength and the bandwidth of the Ti:sapphire are well known, this system allows an optimal rate of sampling.

As a test of the technique and of the experimental setup, we measured the nonlinear response $\Xi^{(2)}(\omega_2, \omega_3)$ of $AgGaS_2$, a birefringent crystal that can be phase matched for mid-infrared generation through difference-frequency mixing. The crystal is cut at $\phi = 45°$ and $\theta = 47°$ for type II phase matching. In this case the nonlinear response is

$$\Xi^{(2)}(\omega_2, \omega_3) = \exp[ik_o(\omega_1)L]\,\frac{\omega_1^2}{4c^2k_o(\omega_1)} \times \chi^{(2)}(-\omega_1; \omega_3, -\omega_2)\left[\frac{\exp(i\Delta kL) - 1}{\Delta k}\right], \quad (3)$$

where $k_{e(0)}(\omega_j)$ is the amplitude of the wave vector at the frequency ω_j along the extraordinary (ordinary)

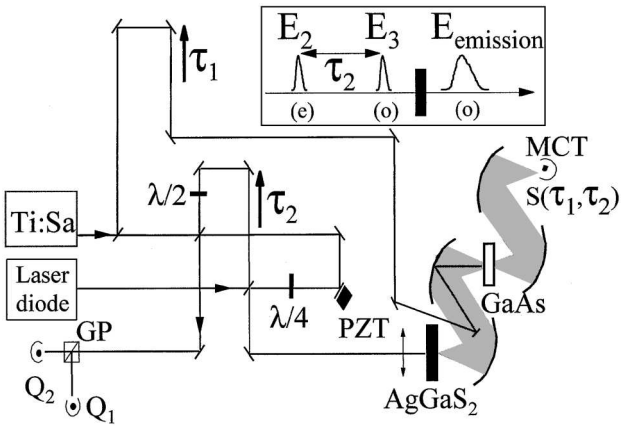

Fig. 1. Experimental layout: Black rectangle, 500-μm-thick $AgGaS_2$ sample ($\phi = 45°$, $\theta = 47°$); white rectangle, 100-μm-thick $\langle 1\bar{1}0 \rangle$ GaAs sample; PZT, piezoelectric transducer; GP, Glan polarizer; MCT, mercury cadmium telluride infrared detector; Q_i, τ_i, see text. Inset, polarizations of the exciting visible pulse sequence and the emitted mid-infrared field.

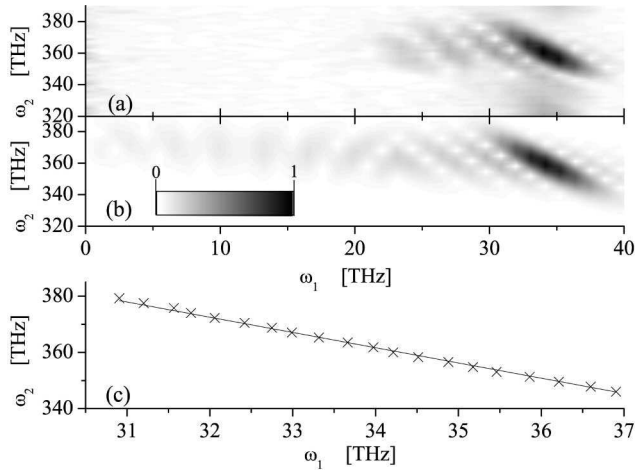

Fig. 2. (a) $|\Xi^{(2)}(\omega_2, \omega_1)E_1(\omega_1)E_2(\omega_2)E_3(\omega_2 + \omega_1)|$ frequency dependency as determined by a two-dimensional Fourier transform of the experimental data (τ_1 from -426.9 to 426.9 fs in $\delta\tau_1 = 6.67$ fs increments; τ_2 from -285.4 to 285.4 in $\delta\tau_2 = 4\lambda_{\text{diode}}/c \approx 8.9$ fs increments). (b) Theoretical results for $|\Xi^{(2)}(\omega_2, \omega_1)E_1(\omega_1)E_2(\omega_2)E_3(\omega_2 + \omega_1)|$, assuming that E_2 and E_3 are 35-THz Gaussian centered around 375 THz. (c) Comparison between (solid line) the phase-matching slope calculated from the refractive indices of $AgGaS_2$ and (crosses) the experimental maxima of map (a). These maxima are determined through a parabolic fit of cuts of the two-dimensional map for each value of ω_2, which results in a resolution far better than $\delta\omega_1$.

axis and $\Delta k = k_e(\omega_3) - k_o(\omega_2) - k_o(\omega_1)$. For this proof-of-principle experiment, as the crystal has no resonance in the spectral domain under study, $\Xi^{(2)}$ is dominated by the bracketed term of phase matching, which serves as a model two-dimensional nonlinear response.

The two visible exciting pulses are polarized each along one of the crystal axis (see the inset of Fig. 1) so that the mid-infrared emission results from only the cross term we are seeking and not from each individual pulse. Note that the use of different polarizations on the two beams breaks the symmetry between ω_2 and ω_3: Phase matching can be achieved here only when $\omega_3 > \omega_2$. The magnitude of $\Xi^{(2)}(\omega_2, \omega_3)$ is plotted in Fig. 2(a) as a function of $\omega_1 = \omega_3 - \omega_2$ and of ω_2. As expected, the obtained result is dominated by phase matching and exhibits several oscillations of the sinc function.

The $|\Xi^{(2)}(\omega_2, \omega_3)|$ map can be simulated with no adjustable parameter by use of Eq. (3) [see Fig. 2(b)]. The good agreement between theory and experiment [Fig. 2(c)] demonstrates the validity of the technique.

Although the precision of the 10-μm τ_1 interferometer should be more than ten times less critical than the precision of the 800-nm τ_2 interferometer, inaccuracies in τ_1 have measurable effects and result in the aliased ghosts along ω_2 that can be seen in Fig. 2(a). Passive stabilization and control of τ_1 is thus the next step toward analysis of more-complicated samples for retrieval of full real and imaginary information of $\Xi^{(n)}$.

To summarize, multiple-pulse nonlinear spectroscopy disentangles overlapping contributions to a complex emission by spreading them along one or more additional axes, thus characterizing the emitting sample. The retrieved multidimensional map (or its projection) of the nonlinear response gives precious insight into couplings between energy levels. In our demonstration of two-dimensional Fourier-transform visible–infrared measurement of a phase-matched $AgGaS_2$ sample, we took special care to ensure accurate and optimal sampling of our temporal data. This technique could be useful for understanding a molecular system such as a protein complex in which electronic (visible) excitation of an optically active cofactor sets vibrational dipoles in a coherent oscillation.[15] It might also prove especially enlightening in the study of quantum wells in which the one dimension of visible frequencies is related to the interband transitions (hence to the wave vector), whereas emission that is due to intersubband transitions is along the other axis in the infrared spectral domain.

We acknowledge the decisive assistance of X. Solinas in the fabrication of the fringe-counting device and thank B. Bousquet, L. Canioni, and J.-P. Likforman for the original phase-locking system. We are grateful to G. Guelachvili for suggesting the dual-quadrature fringe-counting technique used in the experiment. We also thank James Fraser for his critical reading of the manuscript. N. Belabas's e-mail address is nadia.belabas@polytechnique.org.

References

1. L. Lepetit and M. Joffre, Opt. Lett. **21,** 564 (1996).
2. A. Tokmakoff, M. J. Lang, D. S. Larsen, G. R. Fleming, V. Chernyak, and S. Mukemel, Phys. Rev. Lett. **79,** 2702 (1997).
3. O. Golonzka, M. Khalil, N. Dermidöven, and A. Tokmakoff, Phys. Rev. Lett. **86,** 2154 (2001).
4. W. Zhao and J. C. Wright, Phys. Rev. Lett. **84,** 1411 (2000).
5. M. C. Asplund, M. T. Zanni, and R. M. Hochstrasser, Proc. Natl. Acad. Sci. USA **97,** 8219 (2000).
6. P. Hamm, M. Lim, W. F. DeGrado, and R. M. Hochstrasser, Proc. Natl. Acad. Sci. USA **96,** 2036 (1999).
7. J. D. Hybl, A. A. Ferro, and D. M. Jonas, J. Chem. Phys. **115,** 6606 (2001).
8. R. R. Ernst, G. Bodenhausen, and A. Wokaun, *Principles of Nuclear Magnetic Resonance in One and Two Dimensions* (Oxford U. Press, Oxford, 1997).
9. L. Lepetit, G. Cheriaux, and M. Joffre, J. Opt. Soc. Am. B **12,** 2467 (1995).
10. A. W. Albrecht Ferro, J. D. Hybl, S. M. Gallagher Faeder, and D. M. Jonas, J. Chem. Phys. **111,** 10934 (1999).
11. C. Dorrer, N. Belabas, J.-P. Likforman, and M. Joffre, J. Opt. Soc. Am. B **17,** 1795 (2000).
12. A. Bonvalet, J. Nagle, V. Berger, A. Migus, J.-L. Martin, and M. Joffre, Phys. Rev. Lett. **76,** 4392 (1996).
13. N. Belabas, J.-P. Likforman, L. Canioni, B. Bousquet, and M. Joffre, Opt. Lett. **26,** 743 (2001).
14. K. Naganuma, K. Mogi, and H. Yanada, IEEE J. Quantum Electron. **25,** 1225 (1989).
15. M.-L. Groot, M. H. Vos, I. Schlichting, F. van Mourik, M. Joffre, J.-C. Lanbry, and J.-L. Martin, Proc. Natl. Acad. Sci. USA **99,** 1323 (2002).